Available online at www.sciencedirect.com
ScienceDirect
Cement and Concrete Research 36 (2006) 1533–1541
Cement and Concrete Research

Petrographic evidence of calcium oxychloride formation in mortars exposed to magnesium chloride solution

Lawrence Sutter [a], Karl Peterson [a,*], Sayward Touton [a], Tom Van Dam [a], Dan Johnston [b]

[a] Michigan Tech Transportation Institute, 1400 Townsend Dr. Houghton, MI 49931, USA
[b] South Dakota Department of Transportation, 700 E. Broadway Ave., Pierre, SD 57501, USA

Received 1 September 2005; accepted 28 May 2006

Abstract

Many researchers have reported chemical interactions between $CaCl_2$ and $MgCl_2$ solutions and hardened Portland cement paste. One potentially destructive phase reported in the literature is calcium oxychloride ($3CaO{\cdot}CaCl_2{\cdot}15H_2O$). In the past, limited numbers of researchers have reported identification of this phase by X-ray diffraction. In this work, petrographic evidence of oxychloride formation is presented based on optical microscopy, scanning electron microscopy and microanalysis. This evidence indicates that calcium oxychloride does form in mortars exposed to $MgCl_2$ solutions.

Keywords: Magnesium chloride; Deicer salts; Petrography; SEM; EDX

1. Introduction

Keeping roads safe and passable are key concerns during the winter season when ice and snow accumulation on roads and bridges can create hazardous driving conditions. Currently, various chemicals are used for deicing and anti-icing including aqueous solutions of common chlorides (e.g. magnesium chloride, sodium chloride, and calcium chloride) or other chemicals such as calcium magnesium acetate (CMA) or urea. Use of these chemicals has increased given their relatively low cost, ease of use, and effectiveness for deicing and anti-icing. However, the possible detrimental effects of these chemicals on concrete in transportation structures have not been fully examined and documented.

2. Previous work

The application of highly concentrated chloride solutions (e.g. 25% salt by weight) to pavements and bridges results in an increased concentration of dissociated calcium and magnesium ions in the concrete pore water. These free ions are available to combine with compounds in the concrete to form phases such as brucite or magnesium silicate hydrate which may cause expansion or softening. Of course, the dissociation of chlorides into ionic species also increases the concentration of chloride in the pore water solution, which has been documented as a primary cause of corrosion of reinforcing steel. Additionally, the chloride can react with the hardened cement paste causing formation of new products that may be expansive. One such phase is calcium oxychloride.

Reports of oxychloride formation in concrete have primarily come from concrete or mortars exposed to $CaCl_2$ solutions [1]. Collepardi et al. cited a number of studies that have concluded that $CaCl_2$ is associated with the formation of hydrated calcium oxychloride according to the following reaction [2]:

$$3Ca(OH)_2 + CaCl_2 + 12H_2O \rightarrow 3CaO \cdot CaCl_2 \cdot 15H_2O \qquad (1)$$

The reaction in Eq. (1) proceeds fastest at temperatures just above freezing (4–10 °C) causing rapid formation of calcium oxychloride. This reaction is considered disruptive to the

* Corresponding author.
E-mail addresses: cee@mtu.edu (L. Sutter), cee@mtu.edu (K. Peterson), cee@mtu.edu (S. Touton), cee@mtu.edu (T. Van Dam), Dan.Johnston@state.sd.us (D. Johnston).

0008-8846/$ - see front matter © 2006 Elsevier Ltd. All rights reserved.
doi:10.1016/j.cemconres.2006.05.022

Fig. 1. From left to right: 0.40, 0.50, and 0.60 *w/c* mortar cylinders after 84 days in cold $MgCl_2$ brine. Cylinder dimensions are 50 mm in diameter and 100 mm in height.

concrete matrix because of the hydraulic pressures generated. Collepardi et al. speculate that the damaging nature of this reaction has been masked by corrosion of reinforcing steel and freeze–thaw deterioration of the paste, but state that the chemical degradation that occurs is very detrimental [2]. They also report experimental evidence based on decreasing compressive strength, suggesting that severe deterioration occurred in non-air entrained concrete exposed to $CaCl_2$ deicers even though there was no steel to corrode nor was the concrete subjected to temperatures below freezing.

Monosi and Collepardi reported finding calcium oxychloride phase in deteriorated mortars stored for 2 months in a 30% $CaCl_2$ solution at a temperature of 5 °C [1]. The phase was identified by X-ray diffraction of specimens of the wet hardened cement paste. These researchers reported that X-ray diffraction peaks for calcium oxychloride disappear in samples of dried cement paste, compared to the same specimens fresh from the solution. Additionally, they reported the presence of Friedel's salt ($3CaO{\cdot}Al_2O_3{\cdot}CaCl_2{\cdot}10H_2O$) in the same specimens. [In some geochemistry texts, Friedel's salt is

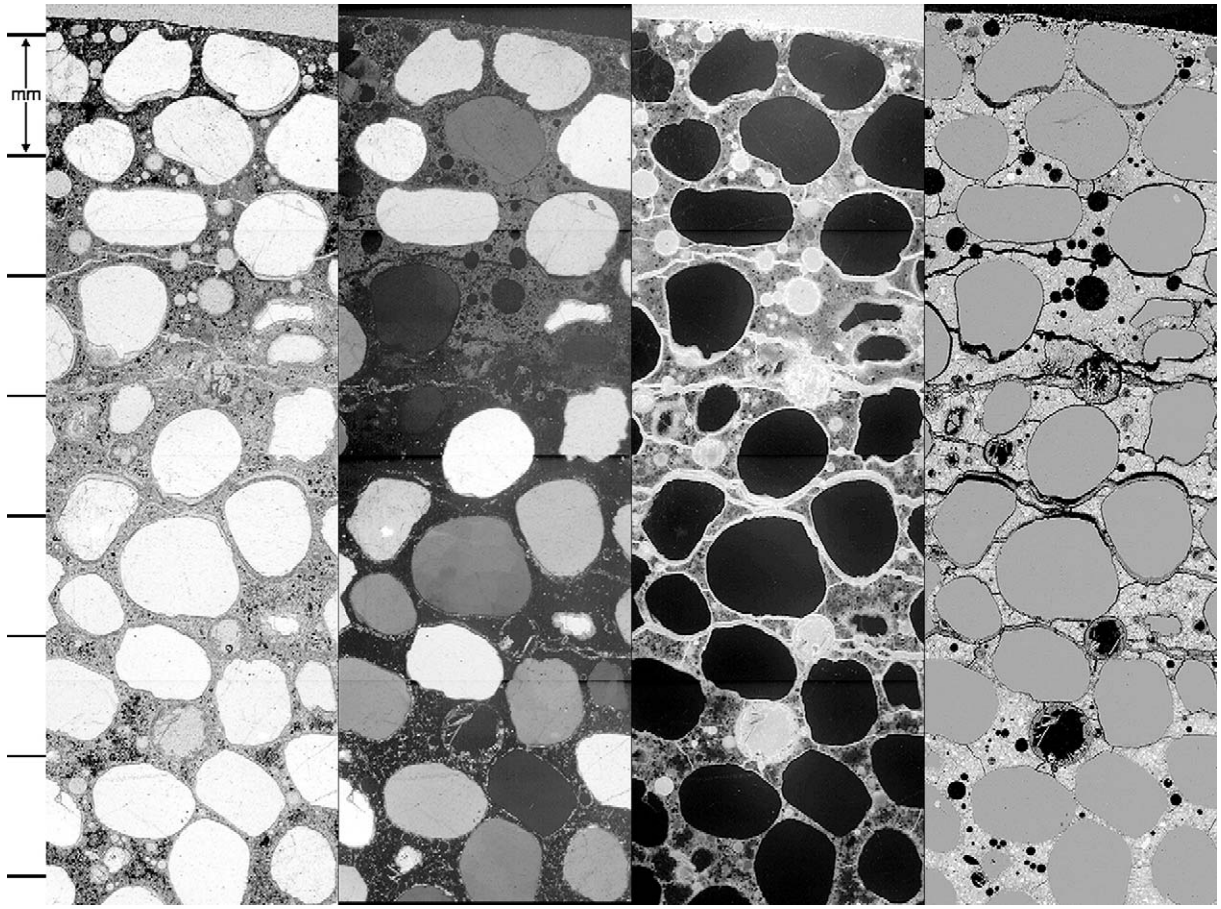

Fig. 2. From left to right: plane polarized, crossed polars, epifluorescent mode, and BSE images. Tic marks along the lefthand side are at 1 mm intervals.

alternatively described by the formula $Ca_2Al(OH)_6[C_{1-x}(OH)_x]\bullet 3H_2O$]. To further investigate the issue, Monosi and Collepardi synthesized calcium oxychloride [1]. Based on X-ray diffraction, they reported that upon drying of the synthesized sample, oxychloride reverts to $CaO{\cdot}CaCl_2{\cdot}2H_2O$. Portlandite peaks were absent from the X-ray diffraction patterns, leading these researchers to suggest that portlandite was consumed during the formation of calcium oxychloride according reaction shown in Eq. (1).

Demediuk et al. report calcium oxychloride as $3CaO{\cdot}CaCl_2{\cdot}xH_2O$ where x can vary from 8 to 13 without affecting the structure [3]. Brown and Bothe report the common forms of calcium oxychloride as being $3CaO{\cdot}CaCl_2{\cdot}12H_2O$ and $3CaO{\cdot}CaCl_2{\cdot}xH_2O$ where x is 10, 11, or 13 depending upon temperature [4]. Brown and Bothe also report a calcium oxychloride form of $CaO{\cdot}CaCl_2{\cdot}H_2O$ as being common.

Abate and Scheetz include calcium oxychloride in their determination of phase equilibria of the $CaO–Al_2O_3–CaCl_2–H_2O$ system, along with Friedel's salt, gibbsite, portlandite, and antarcticite [5]. Although not included in their model, they discuss the role of carbonation, and the likely possibility of the incorporation of CO_3^{2-} in some of the phases. Brown and Bothe studied the same system in the context of phases likely to bind chloride in cement systems. Interestingly, these researchers report that the oxychloride formed in Eq. (1), and Friedel's Salt, do not coexist in equilibrium [4].

Two commonly accepted mechanism for concrete degradation, as a result of magnesium chloride exposure, is shown below in Eqs. (2) and (3).

$$Ca(OH)_2 + MgCl_2 \rightarrow Mg(OH)_2 + CaCl_2 \quad (2)$$

$$C–S–H + MgCl_2 \rightarrow M–S–H + CaCl_2 \quad (3)$$

In addition to the conversion of portlandite to brucite, Eq. (2) could also play a role in oxychloride formation by providing the necessary $CaCl_2$ required for the reaction shown in Eq. (1). It should also be noted that Eq. (2) also results in a decrease in pH from approximately 12.6 to less than 9.

3. Experimental

Three different mortar mixtures were tested in various deicing solutions to examine how these chemicals interact with hardened Portland cement paste. The mortar mixtures were prepared using Ottawa sand, Type I cement, and water. The *w/c* was the independent variable with increments of 0.40, 0.50, and 0.60. The paste volume was held constant for all mixture designs. The cylinders were cured in lime baths for 28 days, and then placed in a temperature control room at 4 °C until deicer exposure testing began.

For testing, mortar cylinders were stored in a 15 wt.% $MgCl_2$ solution at 4 °C for 84 days. The cylinders were then

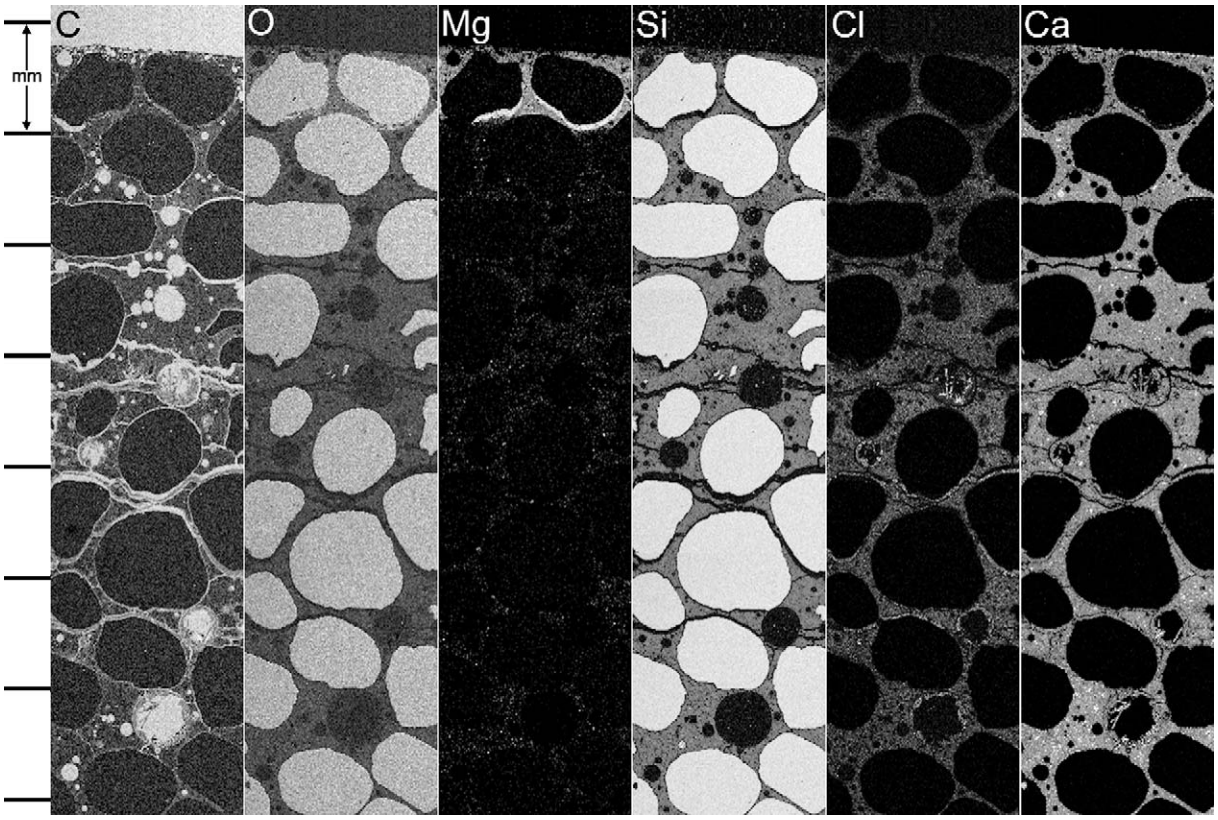

Fig. 3. Elemental maps from area shown in Fig. 2. From left to right: carbon, oxygen, magnesium, silicon, chlorine, and calcium. Brighter regions indicate higher counts for each element.

removed from the solution and stored at room conditions for three months. A 0.50 *w/c* cylinder selected randomly for petrographic analysis was vacuum impregnated with fluorescent epoxy. Thin sections were prepared using water free methods similar to those described by Walker [6]. The final thickness of the thin sections was 30 μm, and the final polish was completed with 0.25 μm diamond grit. The thin sections were examined with an Olympus BX-60 petrographic microscope equipped for epifluorescent illumination. Next, the thin sections were carbon coated and examined in high vacuum mode with a Philips XL40 environmental scanning electron microscope (ESEM) equipped with an EDAX Phoenix Super Ultra Thin Window Energy Dispersive Spectrometer.

Quantitative X-ray energy dispersive spectrometry (EDX) was performed using mineral standards. As a first approximation, 0.2 wt.% oxide is assumed as the detection limit for all oxide phases analyzed. Water and carbonate content were not determined by EDX, but calculated using an iterative mineral recalculation method based on principles outlined by Droop [7]. The method used in this paper begins with the standard conversion of wt.% oxide values to an anion basis, and normalization to a fixed number of anions as outlined by Deer et al. [8]. For example, in this paper, to recast oxide wt.% data into the formula for $3CaO{\cdot}CaCl_2{\cdot}15H_2O$ a fixed number of 20 oxygen anions was used. This initial step in the mineral recalculation resulted in an overestimate of the number of non-hydrogen cations since H^+ was neglected (due to the lack of H_2O in the wt.% oxide input). To estimate water content, a fixed cation approach was used. In the case of $3CaO{\cdot}CaCl_2{\cdot}15H_2O$, wt.% H_2O input values were iterated to solve for a fixed non-hydrogen cation number of four. For the minerals considered in this paper, the non-hydrogen cations are not strictly associated with oxygen, but may also be associated with chloride or other anions such as sulfate and carbonate. To estimate carbonate content, a fixed anion approach was used. In the case of $3CaO{\cdot}CaCl_2{\cdot}15H_2O$, wt.% CO_3^{2-} input values were iterated to solve for a fixed non-oxygen anion number of one. Technically, there are two chloride anions per calcium in $3CaO{\cdot}CaCl_2{\cdot}15H_2O$, but the net charge of two chloride anions is the equivalent of one oxygen anion, hence the fixed value of one. Using this iterative method, water and carbonate contents were assigned stoichiometrically to the wt.% analyses by a fixed ion approach.

4. Results

4.1. Macroscopic observations

Fig. 1 shows the appearance of representative 0.40, 0.50, and 0.60 *w/c* cylinders after 84 days in the cold $MgCl_2$ brine

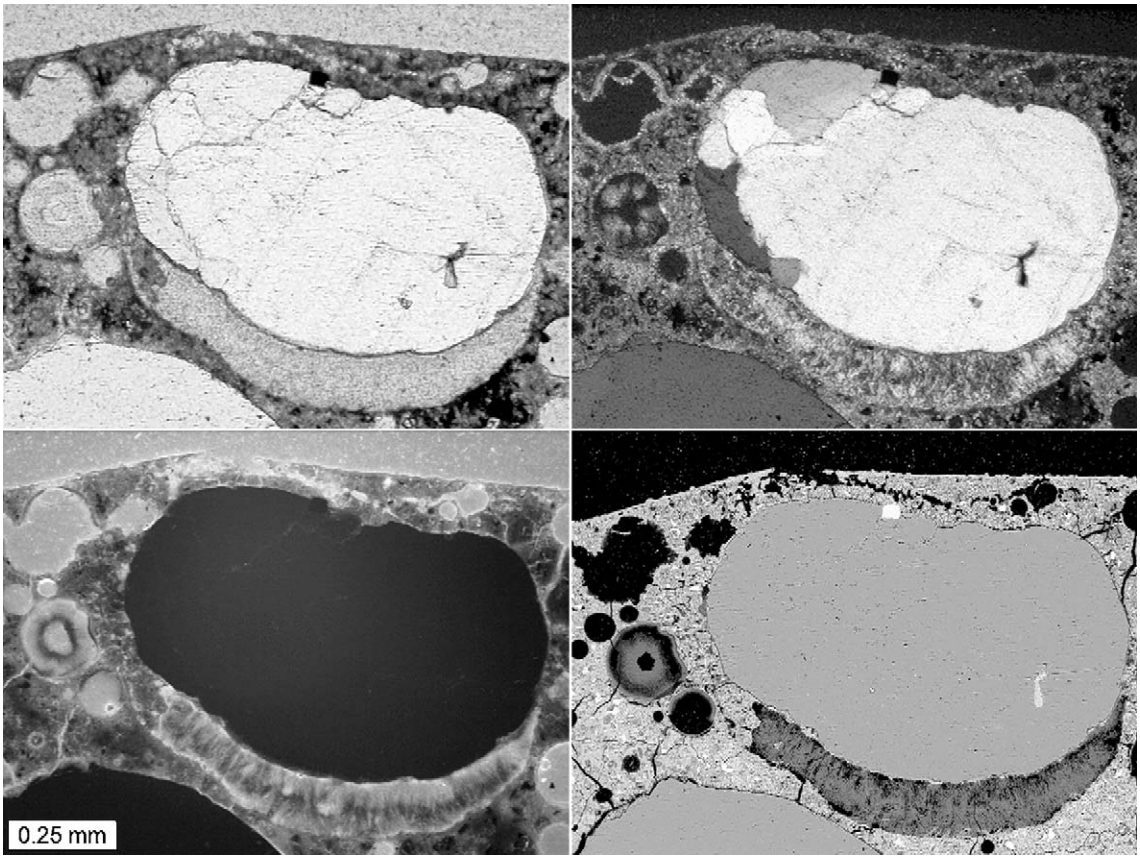

Fig. 4. Fibrous crystals fill crack beneath sand grain, and line air void to left of sand grain. Clockwise from upper left hand corner: plane polarized, crossed polars, BSE, and epifluorescent images.

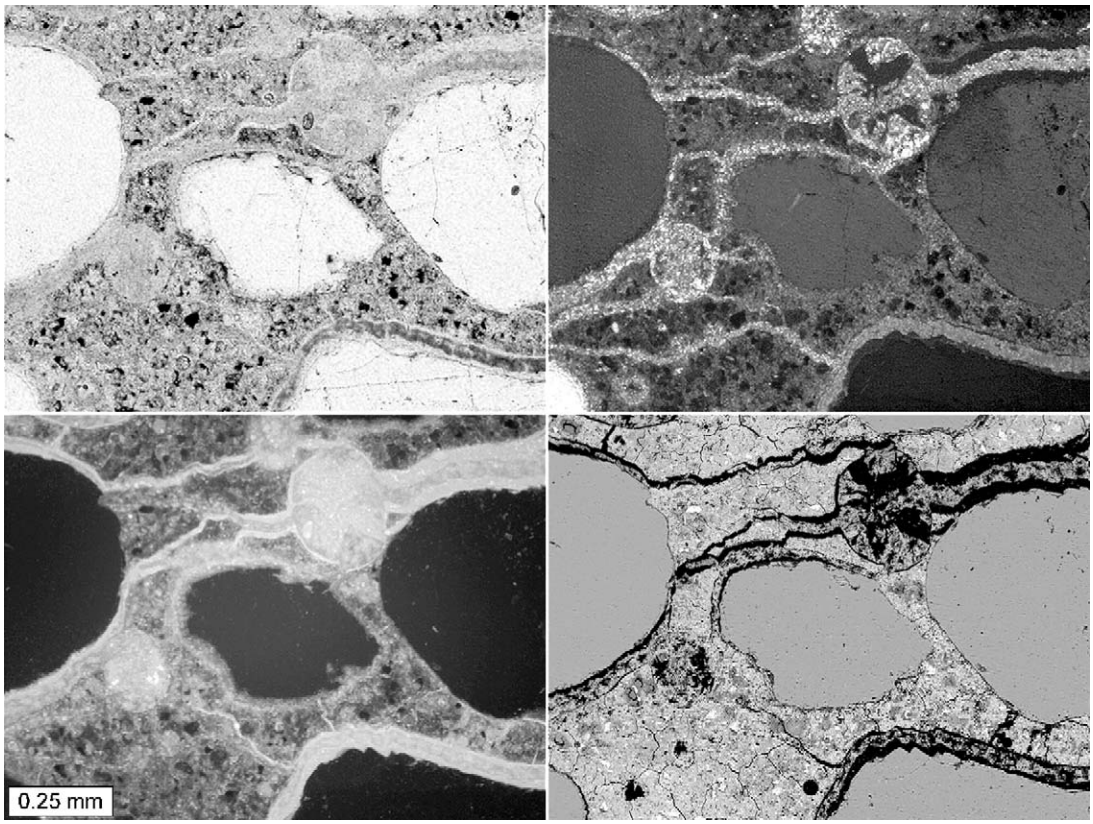

Fig. 5. Typical birefringent crystals in cracks and voids near carbonated zone. Clockwise from upper left hand corner: plane polarized, crossed polars, BSE, and epifluorescent images.

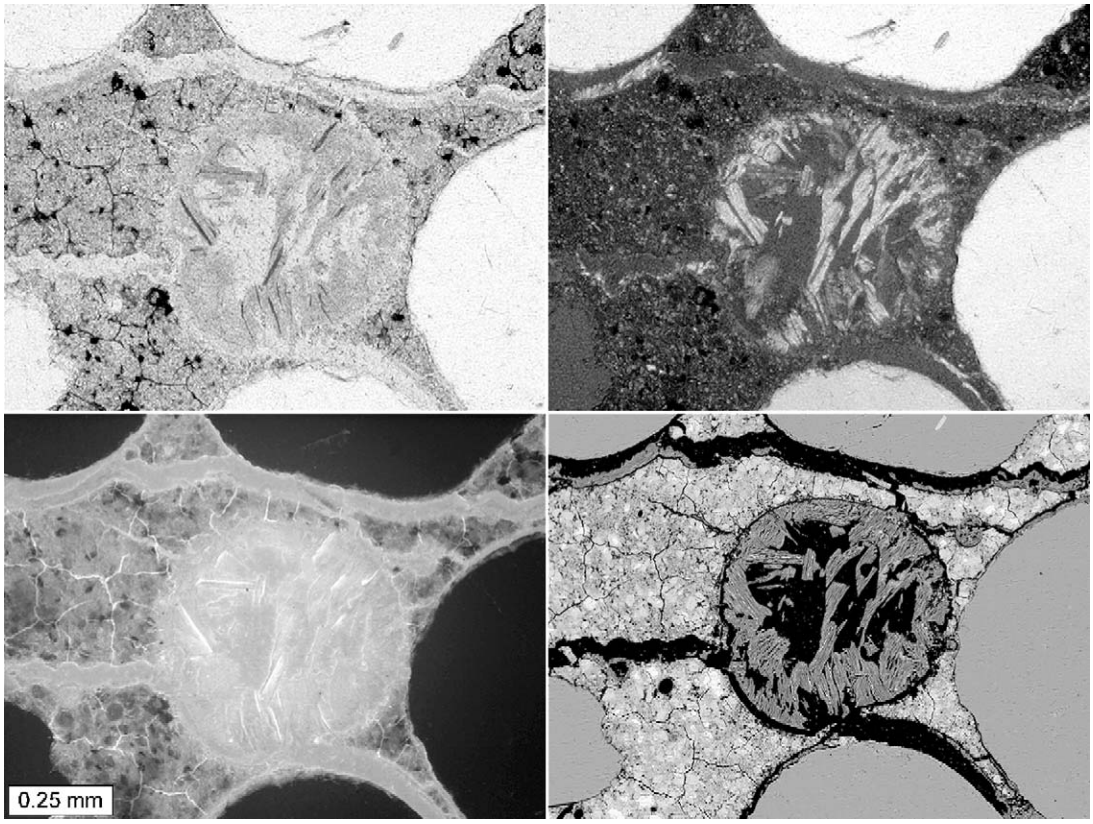

Fig. 6. Typical platey crystals in cracks and voids near advancing front of deterioration. Clockwise from upper left hand corner: plane polarized, crossed polars, BSE, and epifluorescent images.

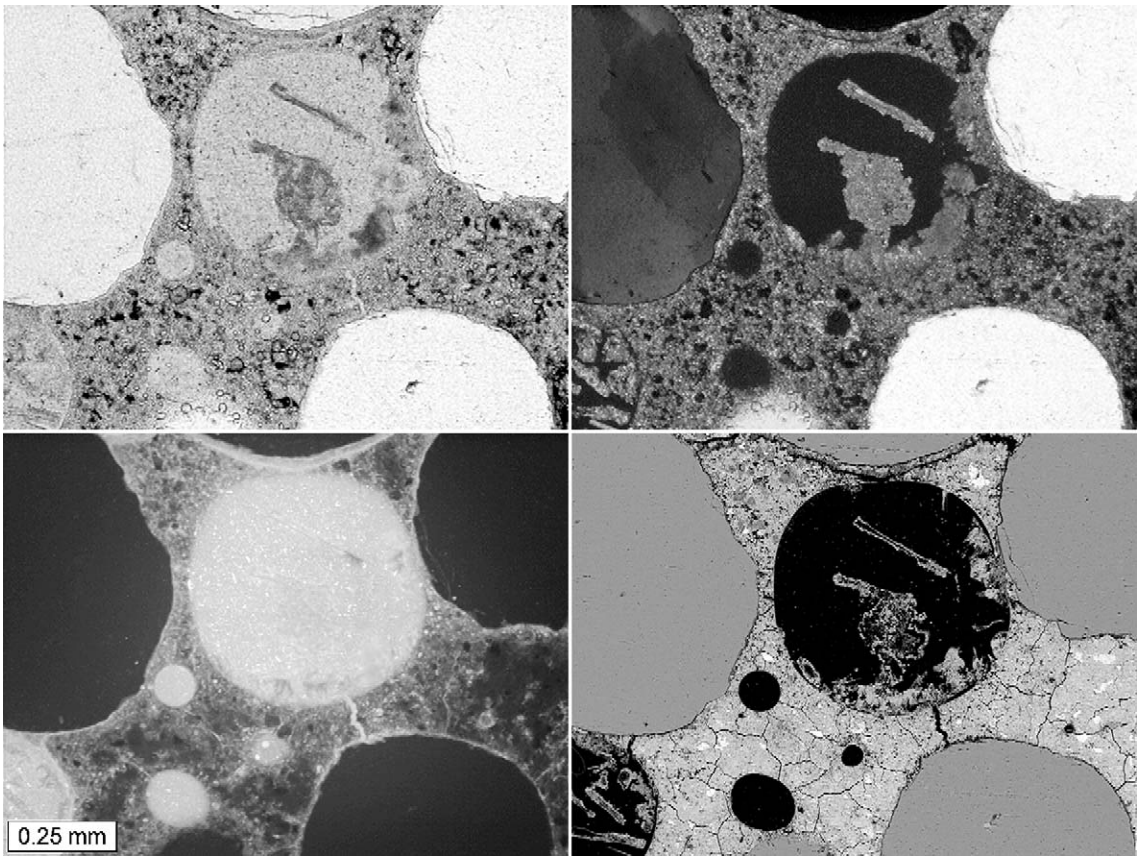

Fig. 7. Pseudomorphs after replacement of secondary portlandite crystals in air void. Clockwise from upper left hand corner: plane polarized, crossed polars, BSE, and epifluorescent images.

solution. The cylinders show clear signs of cracking and expansion.

4.2. Microscope observations

Fig. 2 shows petrographic microscope images, and a back scattered electron (BSE) image to depict the deterioration of a 0.50 *w/c* cylinder in cross section. The orientation of the section is parallel to the top surface of the cylinder, at a depth of approximately 2 cm. The cracks run subparallel to the exterior of the cylinder in concentric rings. In the crossed polar image (second from the left) the depth of carbonation appears to be about 3 mm. The cracks in the carbonated zone appear empty. Just beneath the carbonated zone, the cracks are filled with birefringent crystals. In the crossed polar image, at a depth of 3–5 mm, the cement paste has a dark appearance due to portlandite depletion. At depths greater than 5 mm, portlandite is still present, giving the cement paste a bright

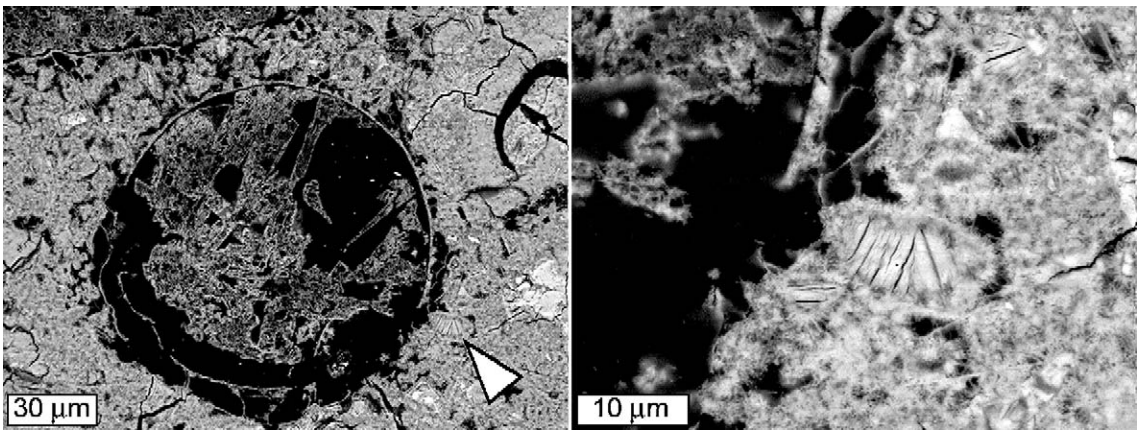

Fig. 8. BSE images of small platey crystals within cement paste. Right hand side image shows close up view of the same platey crystal indicated by the white arrow in the left-hand side image.

Table 1
Summary of EDX measurements from crystal phases depicted in Figs. 4–8 compared to ideal mineral compositions

Element (wt.%)	Measurements from fibrous crystals in magnesium enriched zone (as in Fig. 4) compared to brucite			Measurements from crystals in air voids and cracks near the carbonated zone (as in Figs. 5 and 7) compared to calcium oxychloride with 15 waters			Measurements from large platey crystals in air voids and cracks near the advancing front of deterioration (as in Fig. 6) compared to calcium oxychloride with 12 waters			Measurements from small platey crystals within cement paste (as in Fig. 8) compared to Friedel's salt		
	Avg	SD	Brucite	Avg	SD	Oxychloride	Avg	SD	Oxychloride	Avg	SD	Friedel's salt
Si	0.2	0.03	–	0.1	0.05	–	0.1	0.05	–	0.3	0.17	–
Al	0.0	0.02	–	0.0	0.03	–	0.0	0.03	–	9.2	0.50	9.6
Fe	0.0	0.03	–	0.1	0.08	–	0.1	0.05	–	1.3	0.91	–
Mn	0.0	0.06	–	0.0	0.04	–	0.1	0.06	–	0.1	0.08	–
Mg	39.1	1.65	41.7	0.1	0.03	–	0.1	0.03	–	0.1	0.16	–
Ca	3.0	0.45	–	28.0	3.50	29.2	33.0	1.95	32.4	31.8	1.17	28.6
Na	0.4	0.08	–	0.1	0.06	–	0.0	0.04	–	0.0	0.04	–
K	0.0	0.02	–	0.0	0.04	–	0.0	0.03	–	0.0	0.02	–
S	0.0	0.03	–	0.1	0.08	–	0.0	0.03	–	0.2	0.10	–
Cl	1.4	0.34	–	2.5	0.68	12.9	12.2	1.24	14.3	11.7	0.55	12.6
C [a]	0.0	0.00	–	0.2	0.04	–	0.0	0.02	–	0.0	0.01	–
O [a]	54.0	2.24	54.9	56.3	7.21	52.4	51.4	3.04	48.4	51.6	1.69	45.6
H [a]	3.4	0.14	3.5	5.7	0.72	5.5	5.1	0.30	4.9	4.0	0.13	3.6
Sum	101.6	3.77	100.0	93.2	11.00	100.0	102.1	5.87	100.0	110.5	3.65	100.0

[a] Not included in EDX, determined stoichiometrically.

speckled appearance under crossed polars. Also, at a depth of 3–6 mm, birefringent crystals can be seen in the cracks and in large air voids.

Fig. 3 shows elemental maps made from the same region depicted in Fig. 2. The cracks can be clearly seen in the map of carbon due to the carbon present in the epoxy used to stabilize the sample prior to sectioning. The map for magnesium shows that magnesium from the brine has penetrated into the mortar to a depth of 0.5–0.6 mm. Cracks, filled with magnesium rich deposits, exist beneath the two large sand grains near the surface. The map for chlorine shows that the birefringent crystals in the cracks and air voids at depths of 3–6 mm contain significant amounts of chlorine. The map for calcium shows that the birefringent crystals in the cracks and air voids also contain significant amounts of calcium.

Fig. 4 shows petrographic and BSE images of the magnesium enriched zone in a region similar to the magnesium enriched zone shown in Fig. 3. In Fig. 4, fibrous crystals fill the crack beneath the sand grain, and also line a small air void to the left of the sand grain. Figs. 5 and 6 show examples of the

Table 2
Summary of EDX measurements from crystal phases depicted in Figs. 4–8 recast as mineral formulas and compared to ideal mineral formulas

Ions	Measurements from fibrous crystals in magnesium enriched zone (see Fig. 4) recast as mineral formula based on 2 anions (as per brucite)			Measurements from crystals in the air voids and cracks near carbonated zone (see Figs. 5 and 7) recast as mineral formula based on 20 anions, (as per calcium oxychloride with 15 waters)			Measurements from large platey crystals in air voids and cracks near the advancing front of deterioration (see Fig. 6) recast as mineral formula based on 17 anions, (as per calcium oxychloride with 12 waters)			Measurements from small platey crystals within cement paste (see Fig. 8) recast as mineral formula based on 18 anions, (as per Friedel's salt)		
	Avg	SD	Brucite	Avg	SD	Oxychloride	Avg	SD	Oxychloride	Avg	SD	Friedel's salt
$Si^{(4+)}$	0.0	0.00	–	0.0	0.01	–	0.0	0.01	–	0.1	0.03	–
$Al^{(3+)}$	0.0	0.00	–	0.0	0.01	–	0.0	0.01	–	1.7	0.09	2
$Fe^{(3+)}$	0.0	0.00	–	0.0	0.01	–	0.0	0.01	–	0.1	0.08	–
$Mn^{(2+)}$	0.0	0.00	–	0.0	0.01	–	0.0	0.01	–	0.0	0.01	–
$Mg^{(2+)}$	0.9	0.01	1	0.0	0.01	–	0.0	0.00	–	0.0	0.04	–
$Ca^{(2+)}$	0.0	0.01	–	3.9	0.03	4	3.9	0.02	4	4.0	0.07	4
$Na^{(1+)}$	0.0	0.00	–	0.0	0.01	–	0.0	0.01	–	0.0	0.01	–
$K^{(1+)}$	0.0	0.00	–	0.0	0.01	–	0.0	0.00	–	0.0	0.01	–
$SO_4^{(2-)}$	0.0	0.00	–	0.0	0.02	–	0.0	0.01	–	0.0	0.01	–
$Cl^{(1-)}$	0.0	0.01	–	0.4	0.13	2	1.7	0.15	2	1.7	0.06	2
$CO_3^{(2-)}$ [a]	0.0	0.00	–	0.8	0.07	–	0.2	0.08	–	0.1	0.03	–
$O^{(2-)}$ [a]	2.0	0.01	2	18.8	0.06	18	15.2	0.08	15	16.2	0.03	16
$H^{(1+)}$ [a]	2.0	0.01	2	31.5	0.13	30	24.3	0.17	24	20.4	0.07	20

[a] Not included in EDX, determined stoichiometrically.

birefringent crystals found in cracks and air voids beyond the magnesium-enriched zone. Fig. 5 shows the crystals in voids and cracks found just inside the carbonated zone, at depths of 3–4 mm. Fig. 6 shows the microstructure found at depths of 5 mm or greater, near the advancing deterioration front. The crystals in Fig. 6 have a platey appearance, while the crystals in Fig. 5 do not. Fig. 7 shows birefringent crystals, typical of those found near the carbonated zone, but in what appears to be a pseudomorph replacing secondary portlandite crystals in an air void. Fig. 8 shows back scattered electron images of small platey crystals within the cement paste. The small platey crystals in the cement paste are adjacent to a large air void filled with crystals similar to those shown in Figs. 5 and 7.

4.3. Quantitative SEM analysis

Table 1 summarizes EDX measurements from the crystal phases described in Figs. 4–8, and includes comparisons to ideal mineral compositions. Table 2 shows the measurements from Table 1 recast as mineral formulas, and includes comparisons to ideal mineral formulas. For both tables, the results presented summarize ten typical analyses for each phase.

5. Discussion

The petrographic evidence and EDX data presented verify the presence of brucite formation in the outer layers of the specimens, consistent with the accepted mechanisms shown in Eqs. (2) and (3). Based upon mineral recalculations of the EDX data, the mineral formula for this phase is $(Mg, Ca)_{1.0}(OH)_{2.0}$. Further, the results presented in Tables 1 and 2 show evidence of calcium oxychloride formation in the specimen analyzed. The analyses obtained from the various calcium oxychloride phases, when recalculated into mineral compositions, indicate the calcium oxychloride phase from the carbonated zone fits better the $3CaO{\cdot}CaCl_2{\cdot}15H_2O$ form of calcium oxychloride, while the platey calcium oxychloride phase near the advancing front of deterioration fits better the $3CaO{\cdot}CaCl_2{\cdot}12H_2O$ form of calcium oxychloride. The mineral formula computed for the calcium oxychloride phase from the carbonated zone is $2.9CaO{\cdot}0.2CaCl_2{\cdot}0.8CaCO_3{\cdot}15.8H_2O$. The mineral formula computed for the platey calcium oxychloride phase near the advancing front of deterioration is $2.9CaO{\cdot}0.8CaCl_2{\cdot}0.2CaCO_3{\cdot}12.2H_2O$. When performing the mineral recalculations, the formulas were calculated both with and without CO_3^{2-} included. With the exception of the mineral recalculations for brucite, the results with the carbonate ion included in the calculation yielded the best results. It is postulated that in these phases, CO_3^{2-} is substituting to some degree based upon these mineral recalculations and upon X-ray energy dispersive spectra collected from phases where pronounced carbon peaks were observed. The carbon content of these phases was not determined directly due to the inherent problems with performing such analyses on carbon coated specimens by means of EDX. It should be noted that qualitatively, the observed carbon peaks for the carbonated phases were over and above that which would be associated with the carbon coating itself. This observation is based upon comparisons between the carbon peak observed on the calcium oxychloride phases as compared to analyses of unaltered portlandite under the same conditions, on the same sample. EDX results from phases identified as Friedel's salt and the subsequent mineral recalculation presented in Table 2 is for the most part consistent with the ideal form of this phase. The Friedel's salt phase also appears to be carbonated to some degree. The mineral formula computed for the Friedel's salt phase is $3.0CaO{\cdot}0.9CaCl_2{\cdot}0.1CaCO_3{\cdot}0.9Al_2O_3{\cdot}10.2H_2O$.

The results obtained from this specimen and others support the postulation that in the presence of concentrated magnesium chloride solutions, calcium oxychloride will form by the following reactions:

$$Ca(OH)_2 + MgCl_2 \rightarrow Mg(OH)_2 + CaCl_2 \quad (4)$$

$$3Ca(OH)_2 + CaCl_2 + 12H_2O \rightarrow 3CaO \cdot CaCl_2 \cdot 15H_2O \quad (5)$$

The pseudomorph replacing secondary portlandite shown in Fig. 7 is strong evidence in support of the reaction shown in Eq. (5). Exposure to atmosphere creates a carbonated form that appears to be much lower in chlorine content and suggests a solid solution between a pure calcium oxychloride phase and a calcium oxycarbonate phase.

In the process of identifying the oxychloride phases, analyses such as those shown in Tables 1 and 2 were common. After dehydration, it is impossible to unequivocally identify a hydrated species but the cation balance should remain. Additional work is being conducted to confirm the carbonated form of oxychloride but these microanalyses and mineral recalculations tend to confirm its presence in these mortars. In the specimen analyzed, Friedel's salt was also detected. This observation is not consistent with predictions from thermodynamic modeling of the $CaO–Al_2O_3–CaCl_2–H_2O$ system, possibly due to localized disequilibria.

6. Conclusions

Calcium oxychloride forms when mortar specimens are submerged in 15% $MgCl_2$ solution for 84 days. A carbonate substituted form of calcium oxychloride was also identified. Petrographic evidence indicates that these phases form through consumption of portlandite and precipitation in voids in cracks. Direct replacement of portlandite is also suggested by observations of calcium oxychloride pseudomorphs after portlandite crystals in air voids. Friedel's salt was also found in the specimen analyzed indicating that Friedel's salt and calcium oxychloride can occur together in spite of thermodynamic predictions to the contrary.

References

[1] S. Monosi, M. Collepardi, Research on $3CaO{\cdot}CaCl_2{\cdot}15H_2O$ identified in concretes damaged by $CaCl_2$ attack, Il Cimento 87 (1990) 3–8.

[2] M. Collepardi, L. Coppola, C. Pistolesi, Durability of concrete structures exposed to $CaCl_2$ based deicing salts, in: V.M. Malhotra (Ed.), Durability of Concrete ACI SP-145, 3rd CANMET/ACI International Conference, Nice, France, 1994, pp. 107–115.

[3] T. Demediuk, W.F. Cole, H.V. Hueber, Studies on magnesium and calcium oxychlorides, Australian Journal of Chemistry 8 (1955) 2133–2152.
[4] P. Brown, J. Bothe, The system $CaO–Al_2O_3–CaCl_2–H_2O$ at 23°C and the mechanisms of chloride binding in concrete, Cement and Concrete Research 34 (2004) 1549–1553.
[5] C. Abate, B.E. Scheetz, Aqueous phase equilibria in the system $CaO–Al_2O_3–CaCl_2–H_2O$: The significance and stability of Friedel's salt, Journal of the American Ceramic Society 78 (4) (1995) 939–944.
[6] H.N. Walker, Petrographic methods of examining hardened concrete: A petrographic manual, FHWA-RD-97-146, U.S. Department of Transportation, Federal Highway Administration, Research and Development, Turner-Fairbanks Highway Research Center, McLean, Virginia, 1997, http://www.tfhrc.gov/pavement/pccp/petro/index.htm.
[7] G.T.R. Droop, A general equation for estimating Fe^{3+} concentrations in ferromagnesian silicates and oxides from microprobe analyses using stochiometric criteria, Mineralogical Magazine 51 (1987) 431–435.
[8] W.A. Deer, R.A. Howie, J. Zussman, An Introduction to the Rock Forming Minerals, Wiley Publishing, New York, 1992.